Eur. Phys. J. B **35**, 201–207 (2003)
DOI: 10.1140/epjb/e2003-00269-1

THE EUROPEAN PHYSICAL JOURNAL B

Dynamical phase transition in two-dimensional fully frustrated Josephson junction arrays with resistively shunted junction dynamics

M.-B. Luo[a] and Q.-H. Chen

Department of Physics, Zhejiang University, Hangzhou 310027, P.R. China

Received 8 April 2003 / Received in final form 29 May 2003
Published online 2 October 2003 –

Abstract. The dynamical phase transitions in two-dimensional fully frustrated Josephson junction arrays at zero temperature are investigated numerically with the resistively shunted junction model through the fluctuating twist boundary condition. The model is subjected to a driving current with nonzero orthogonal components i_x, i_y parallel to both axes of the square lattice. We find a roughly lattice size independent phase diagram with three dynamical phases: a pinned vortex lattice phase, a moving vortex lattice phase and a moving plastic phase. The phase diagram shows a direct transition from the pinned vortex to the moving vortex phase and the separation of the pinned vortex and the moving plastic phases. The time-dependent voltages v_x and v_y are periodic in the moving vortex lattice phase. But they are aperiodic in the moving plastic phase, resulting in non-monotonic characteristics and hysteresis in the current-voltage curves. It is found that the characteristic frequency is twice the time-averaged voltage in the moving vortex phase and around the time-averaged voltage in the plastic flow regime.

PACS. 64.60.Ht Dynamic critical phenomena – 74.25.Sv Critical currents – 74.25.Fy Transport properties

1 Introduction

Superconducting Josephson junction arrays (JJA) [1] generally consist of superconducting grains embedded in a nonsuperconducting host. Such arrays can be microfabricated with unit cells as small as a few microns on each side in one or two dimensions with 1000 or more junctions on a line. They have attracted considerable interest in the past decade, due to rich equilibrium and non-equilibrium properties [2–8]. The arrays offer excellent models to study transport in some complicated systems, such as high-temperature superconductors, which may contain naturally weak links [9–16]. They are also of practical significance to be employed as millimeter-wave oscillators and amplifiers [17–19].

Much evidence has revealed that vortex lattices in superconductors or Josephson arrays, as well as other ordered systems, can exhibit various dynamical phase transitions, as a function of controllable external parameters, such as driving force and temperature [2,12,15,20–25]. In disordered superconducting films and JJAs, there are at least three distinct phases as a function of driving current at zero temperature. At low driving current, the vortex lattice is pinned and typically shows a glasslike order. At intermediate driving current, the vortex lattice is depinned and starts to move, but the dynamics is dominated by disorder which leads the system into a plastic flow regime. In this regime, the vortices form a pattern of pinned and unpinned regions, often described as an incoherent flow. Finally, at high driving current, disorder would have little effect and the vortex system enters a moving glass, resulting in a coherent vortex motion. The moving vortex lattice is much more ordered and static channels are easily formed. One of the characteristics of the moving glass is the existence of a transverse critical force [26], which has received considerable numerical confirmation [27].

Recently, these three kinds of dynamical phase transitions were also observed in the resistively shunted junction (RSJ) model with a uniform frustration [6]. Fisher *et al.* [6] studied numerically the dynamical phase transitions in a fully frustrated (FF) square JJA subjected to a driving current with nonzero orthogonal components i_x, i_y parallel to both axes of the square lattice. Based on the RSJ model, a dynamical phase diagram with three phases was observed at zero temperature: (A) a pinned vortex lattice with zero time-averaged voltages $\langle v_x \rangle$ and $\langle v_y \rangle$, (B) a moving vortex lattice phase in which only one component of the time-averaged voltages is nonzero, *i.e.* $\langle v_x \rangle = 0$, $\langle v_y \rangle > 0$ or $\langle v_x \rangle > 0$, $\langle v_y \rangle = 0$, and (C) a moving plastic phase in which both $\langle v_x \rangle$ and $\langle v_y \rangle$ are nonzero. The phase diagram depends strongly on the system size, and at low driving currents the plastic phase locates between the pinned and the elastic moving phases.

[a] e-mail: mbluo@hzcnc.com

We notice that some of reference [6]'s results are in contradiction with several previous findings. The dynamical phase diagram is far different from that obtained by the authors themselves from a 2×2 model system, with an approach previously used by Rzchowski *et al.* [10]. The 2×2 system exhibits a direct dynamical phase transition from the pinned vortex lattice phase to the moving vortex lattice phase [6]. On the other hand, the critical current they obtained is smaller than the well-known analytical [28] and experimental [28,29] result, $i_c = (\sqrt{2} - 1)$ in units of the critical current of a single junction. Recently, Kim *et al.* [30] obtained this theoretical critical current with high accuracy in the RSJ model using the fluctuating twist boundary condition (FTBC) where the translational symmetry is conserved [31,32]. The FTBC preserves the natural periodic boundary conditions for the vortices. While the open boundary condition (OBC) taken in reference [6] breaks the periodicity of the vortices along the current direction.

In this paper, we investigate the zero temperature dynamical phase transitions in the 2D FF RSJ model with the FTBC. Starting from an initial ordered state, we find a simple dynamical phase diagram with three dynamical phases, and find it almost independent of the system size. The time-dependent voltages and the corresponding power spectra are also calculated.

The remainder of the paper is organized as follows. Section 2 describes the calculation method, including a brief introduction of FF RSJ model with FTBC. The results are given in Section 3. Finally, Section 4 presents a short summary of our main conclusions.

2 Model and calculation method

Calculations are performed on FF square Josephson junction arrays with RSJ dynamics under FTBC. The FTBC has been first introduced in the equilibrium Monte Carlo simulation [31] and later extended to the RSJ dynamical simulation [13,30,32]. External currents are applied in both x and y directions with the current density $\mathbf{I} = (I_x, I_y)$. At zero temperature, the net current from site i to site j is written as the sum of the supercurrent and the normal resistive current:

$$I_{ij} = I_0 \sin(\theta_i - \theta_j - A_{ij} - \mathbf{r}_{ij} \cdot \mathbf{\Delta}) + \frac{V_{ij}}{R} \qquad (1)$$

where I_0 is the critical current of the single junction, V_{ij} is the voltage drop across the junction, R is the shunt resistance, $A_{ij} \equiv (2e/\hbar) \int_i^j \mathbf{A} \cdot d\mathbf{l}$ is the integral of the vector potential $\mathbf{A}$ from site i to j, and θ_i is the phase angle of the superconducting order parameter on site i and is periodic in both directions ($\theta_i = \theta_{i+L\hat{x}} = \theta_{i+L\hat{y}}$). $\mathbf{r}_{ij} \equiv \mathbf{r}_j - \mathbf{r}_i$ is a unit vector from site i to j, and $\mathbf{\Delta} = (\Delta_x, \Delta_y)$ is the fluctuating twist variable. We assume a constant, uniform external field $\mathbf{B}$ along the z direction, for which the summation of A_{ij} around any unit cell is

$$\sum_{cell} A_{ij} = 2\pi f, \qquad (2)$$

where the constant $f = BS/\Phi_0$ is the density of magnetic flux quanta ($\Phi_0 = h/2e$) per unit cell, and S is the area. $f = 1/2$ for the FF JJA model.

The phase variable θ_i on the site i with position vector $\mathbf{r}_i$ satisfies

$$\dot{\theta}_i = -\sum_j G_{ij} \sum_k{}' [\sin(\theta_j - \theta_k - A_{jk} - \mathbf{r}_{jk} \cdot \mathbf{\Delta})] \qquad (3)$$

where G_{ij} is the lattice Green function, the primed summation is over nearest-neighbor sites (k) of j. The dynamics of $\mathbf{\Delta}$ is given by

$$\frac{d\Delta_x}{dt} = \frac{1}{L^2} \sum_{\langle ij \rangle x} \sin(\theta_i - \theta_j - A_{ij} - \Delta_x) - i_x \qquad (4)$$

$$\frac{d\Delta_y}{dt} = \frac{1}{L^2} \sum_{\langle ij \rangle y} \sin(\theta_i - \theta_j - A_{ij} - \Delta_y) - i_y \qquad (5)$$

where $\sum_{\langle ij \rangle x}$ and $\sum_{\langle ij \rangle y}$ denote the summation over all links in the x direction and y direction, respectively, and the current densities $i_x \equiv I_x/I_0$, $i_y \equiv I_y/I_0$ are in units of I_0. Here the unit of time is $\hbar/2eRI_0$. The voltage drops across the system in the x and y directions read

$$V_x = -L\dot{\Delta}_x \qquad (6)$$

and

$$V_y = -L\dot{\Delta}_y \qquad (7)$$

respectively, where the voltages are in units of RI_0. The voltages V_x and V_y are dependent on the system size L for a given current density. Therefore, in this work, we calculate the mean voltage drops per lattice constant $v_x = V_x/L$ and $v_y = V_y/L$ instead. For convenience, units are taken of $I_0 = R = \hbar/2e = 1$ in the following.

In the present calculation, uniform external currents are fed into the system. Our runs start from an initial ordered state: all phase differences $\phi_{ij} = \theta_i - \theta_j - A_{ij} = \pm\frac{\pi}{4}$ corresponding to the zero-current equilibrium ground state and the fluctuating twist variable $\mathbf{\Delta} = (0, 0)$. The ground state is a "checkerboard" vortex lattice, in which a vortex sits in every other site of a square grid. The dynamic equations (3), (4) and (5) are solved with a second-order Runge-Kutta algorithm. The time step is chosen as $\Delta t = 0.05$ except where mentioned. And a pseudo-spectral algorithm [33] is used to accelerate the calculation.

The time-averaged voltages $\langle v_x \rangle$ and $\langle v_y \rangle$ are calculated over a long time scale after reaching a steady-state. To determine the steady-state, we have checked $\langle v_x \rangle$ and $\langle v_y \rangle$ for every $(2^n - 2^{n-1})$ time interval. In pinned vortex and moving vortex phases, the system usually reaches its steady state before $n = 10$. Therefore, in these two phases we typically discard the first 2^{10} steps and use the subsequent 2^{10} steps for measuring the voltages. In the plastic phase, however, we find that it is quite time-consuming to reach the steady state: the time-averaged voltages often vary with n. Nevertheless, we find that the fluctuation of the voltage is less than 1% for most cases when $n \geq 20$. In order to determine the steady state automatically, we discard the first 2^{18} (~ 4000) time steps, and record the mean

voltages $\langle v_x \rangle$ and $\langle v_y \rangle$ for every $n \geq 19$. After $n = 20$, the fluctuations of the mean voltages are calculated as

$$\delta v_k = \left| \frac{\langle v \rangle_n - \langle v \rangle_{n-k}}{\langle v \rangle_n} \right| \tag{8}$$

for both $\langle v_x \rangle$ and $\langle v_y \rangle$ with $k = 1$ and 2. We assume that the system reaches its steady state when both δv_1 and δv_2 are less than 0.5% simultaneously for the voltages $\langle v_x \rangle$ and $\langle v_y \rangle$. Once this criterion is satisfied, we reckon the $\langle v_x \rangle_n$ and $\langle v_y \rangle_n$ are the final estimates of the voltages.

For real superconducting JJAs, the situation will be more complex than a simple XY model. One should also be careful about the self induced field effects [34]. To take account of the self induced field effects generated by a "screening current", one should use a more complex model, like the Nakajima-Sawada (NS) model [34]. The NS model is more realistic and will result in a richer dynamics than a simple XY model, but it is more complicated and difficult to solve. The present results will be modified if the self induced field effects are included, but the basic physics might remain unchanged. On the other hand, at zero-temperature, without the thermally activated vortices and antivortices, the intrinsic length scale related the separation of the bound vortex pairs [35] is lacking, so the present study does not suffer from the finite-size effect, which will be confirmed in the next section.

3 Results and discussions

Current dependent voltages $\langle v_x \rangle$ and $\langle v_y \rangle$ are calculated for the square FF RSJ model without disorder at zero temperature. We find that the voltages $\langle v_x \rangle$ and $\langle v_y \rangle$ are almost independent of the system size ranging from 2×2 to 128×128. Therefore, the phase diagram is also roughly independent of the system size. In the present work, we use a moderate system size of 32×32.

Figure 1 shows the dynamical phase diagram for the FF RSJ model at zero temperature as function of the currents in both directions. Analogous to reference [6], three different phases are found: (A) a pinned vortex lattice which has zero voltages $\langle v_x \rangle$ and $\langle v_y \rangle$, (B) a moving vortex lattice phase in which only the voltage along one of the principle directions is nonzero, and (C) a moving plastic phase in which both $\langle v_x \rangle$ and $\langle v_y \rangle$ are nonzero. The criterion for the zero voltage is $v = 10^{-3}$. The phase diagram is symmetric around line $i_x = i_y$ due to the symmetry of the system.

However, our phase diagram is different from that of reference [6] in several aspects. First, applying the currents only in one principle direction, we find that the critical current is 0.414, which is consistent with the well-known theoretical and experimental results $i_c = (\sqrt{2} - 1)$. This critical current is almost independent of the system size, analogous to that in the 2D JJA model without frustration ($f = 0$) [2]. Recently, Kim and Minnhagen have presented a detailed discussion about this critical current without the transverse component [30]. They concluded

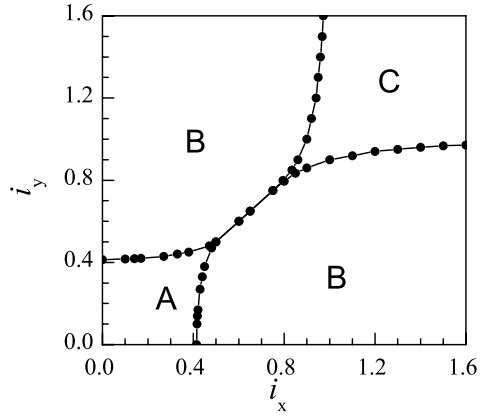

Fig. 1. Dynamic phase diagram for square FF RSJ model with currents applied in both the x and y directions. Region A: pinned vortex lattice ($\langle v_x \rangle = \langle v_y \rangle = 0$). Region B: moving vortex lattice phase ($\langle v_x \rangle = 0$, $\langle v_y \rangle > 0$ or $\langle v_x \rangle > 0$, $\langle v_y \rangle = 0$). Region C: moving plastic phase ($\langle v_x \rangle > 0$, $\langle v_y \rangle > 0$).

that the smaller critical current originates from the uniform injection of external currents under the OBC. Second, the phase diagram is almost independent of the system size in our study, in contrast to that in reference [6]. This discrepancy may also be attributed to the different boundary conditions employed. It is known that the OBC for the phase angles leads to a nonperiodic boundary condition for vortex interactions. The natural condition should be the FTBC where the periodicity for vortices is met and thus the translational symmetry of the ground state is preserved [30]. Finally, we find that the system exhibits a direct dynamical phase transition from the pinned vortex lattice phase to the moving vortex phase at low transverse current, while in reference [6] there is always a plastic phase between the pinned vortex phase and the moving vortex phase. We think that this direct phase transition results from the fact that the translational invariant vortex patterns are the same in the pinned regime and in the elastic moving regime. Similar results are also found by Marconi and Domínguez [15] in JJA with uniform frustration $f = 1/25$ at zero or low temperatures. The uniform current injection under OBC could produce a vortex pattern which is not fully compatible with the translational invariant vortex pattern [30]. This artificially results in a plastic flow regime between the pinned and moving phases. Even with FTBC, if the vortex pattern in the pinned regime is not fully compatible with that in the elastic flow regime, an intermediate plastic flow regime could also appear, which is demonstrated in reference [12] for strongly disordered JJA with $f = 1/25$.

Though there are a lot of differences described above between our phase diagram and that of reference [6] with OBC, we find that the phase diagram is similar to that of a 2×2 model system in reference [6]. The reason for this similarity is that, when $L = 2$, equations (3), (4) and (5) are identical to the dynamics equations for the 2×2 model system employed in reference [6]. Therefore, the 2×2 system is identical to the $L = 2$ RSJ model with FTBC. The similarity is valid also for a large system with

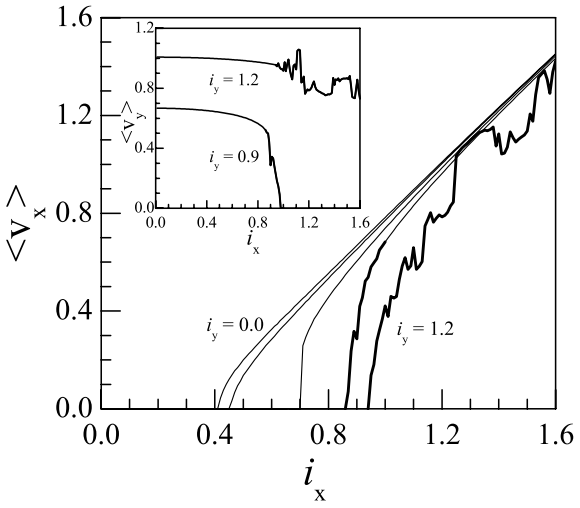

Fig. 2. Current-voltage ($i_x - \langle v_x \rangle$) curves of the square FF RSJ model for different transverse current i_y. From left to right, $i_y = 0.0$, 0.4, 0.7, 0.9, and 1.2. The thick lines represent the system in the plastic phase. The current step $\Delta i = 0.01$ was used in the calculation. The inset shows the $\langle v_y \rangle - i_x$ curves for $i_y = 0.9$ and $i_y = 1.2$.

$L = 2n(2n \times 2n)$, for it can be viewed as n^2 repeated 2×2 arrays. Therefore, it is reasonable to find a size independent phase diagram.

One of the fascinating features of the moving phase is the transverse pinning [26]. We apply the current i_y along the y direction, then the vortex may move along the x direction. The peculiarity of FF RSJ model, one kind of periodic pinning model [15,16], is that the transverse pinning exists even for the current $i_y < i_c$, due to the intrinsic lattice pinning originating from the discretization of the network. Figure 2 shows the current-voltage (IV) curves ($i_x - \langle v_x \rangle$) for various currents i_y ranging from 0 to $i_y \gg i_c$. For $i_y = 0$, we slowly increase i_x from $i_x = 0$. For $i_y > 0$, we first increase i_y from $i_y = 0$ while i_x is fixed to zero, after i_y reaches the given value, we then increase i_x while keeping i_y fixed. In all these calculations, a current step $\Delta i = 0.01$ is used, and the final state of the previous current is used as the initial state of the subsequent current. One can see that the transverse critical current in the x direction i_{xc} increases with the current i_y. This effect is also clearly demonstrated in the inset of Figure 2: $\langle v_y \rangle$ decreases with increasing i_x in the moving vortex phase. It follows that the transverse critical force in the FF JJA model increases as the driven force increases, similar to that in the moving vortex system subject to random disorder [36]. We argue that, besides the effect of the lattice pinning, the transverse critical force in this periodic pinning model might also have a similar origin in the random pinning model, *i.e.* the additional static mode of transverse pinning once the system is set in motion [26], although the detailed theoretical analysis for the periodic pinning is still lacking to date.

In the moving vortex phase, we find that the voltage $\langle v_x \rangle$ increases smoothly with i_x. However, in the plastic phase, there exist some abrupt changes in the voltage $\langle v_x \rangle$

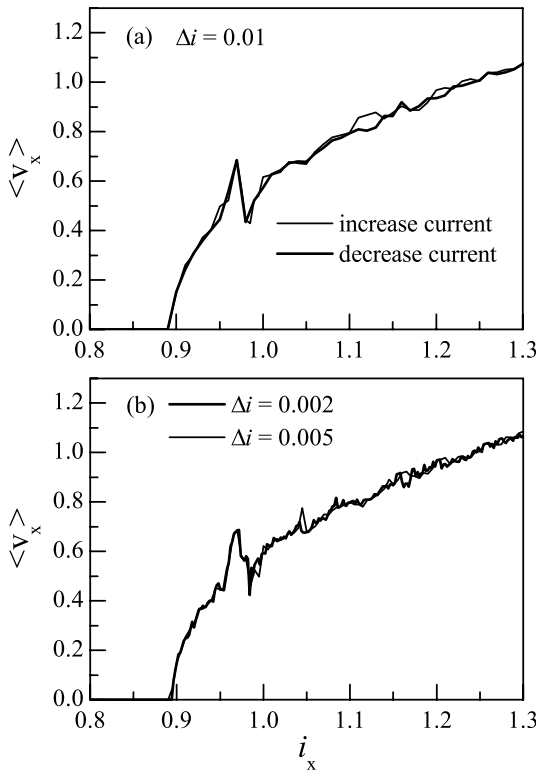

Fig. 3. The non-monotonic current-voltage curves in the moving plastic phase. The current steps are (a) $\Delta i = 0.01$ and (b) $\Delta i = 0.002$ and 0.005. For all calculations i_y is fixed at 0.96.

as well as in $\langle v_y \rangle$, as shown in Figure 2. We find that such non-monotonic characteristics are always present in the plastic flow regime after examining several IV curves with different current steps Δi in the case of $i_y = 0.96$, which are displayed in Figures 3a and b. In addition, we find that the mean voltages $\langle v_x \rangle$ and $\langle v_y \rangle$ are mainly determined by the external current, although small differences still exist for different current steps. It is known that there are typically a number of vortex lattice configurations which are degenerate in energy. If the array sits in one of these configurations, then we will get a certain voltage. The configuration in which the system sits may depend on the initial condition since the final mean voltage depends on the current step Δi. Therefore, it is reasonable to observe the non-monotonic characteristics shown in Figure 2, as well as a hysteresis loop shown in Figure 3a if one ramps up and ramps down the current.

To show the temporal correlation in various moving phases, we calculate the time-dependent voltage and its power spectra

$$S_{x,y}(\omega) = \left| \frac{1}{T} \int_0^T v_{x,y}(t) \exp(-i\omega t) dt \right|^2 \qquad (9)$$

where ω is the angular frequency.

We present the time-dependent voltage $v_{x,y}(t)$ at various $i_y = 0.0$, 0.8, and 1.1 for a given current $i_x = 1.4$ in Figures 4a–c. Here the time step $\Delta t = 0.01$ is used. The

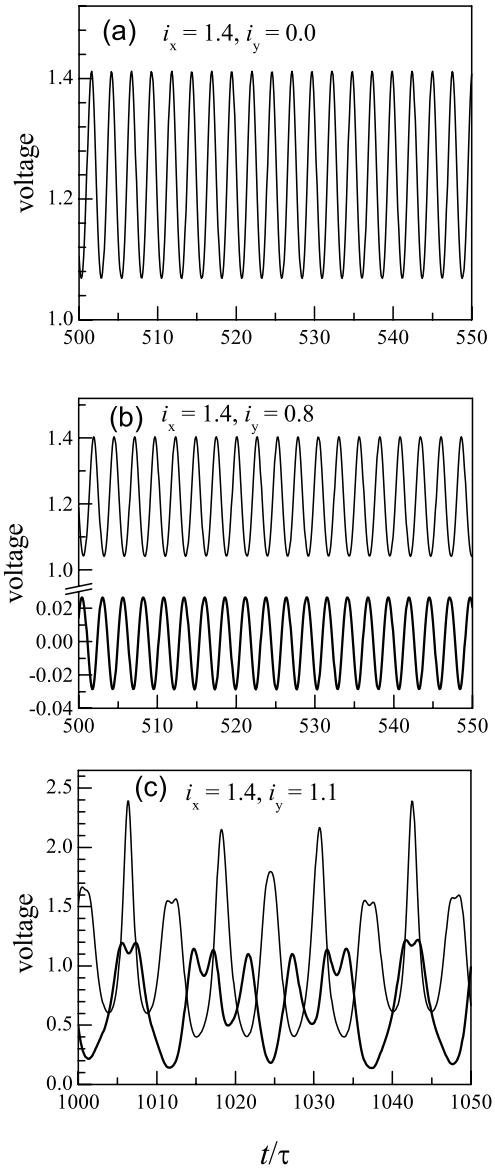

Fig. 4. Time-dependent voltage trace $v_x(t)$ (thin line) and $v_y(t)$ (thick line) at different applied currents: (a) **i**=(1.4,0.0), (b) **i**=(1.4,0.8), and (c) **i**=(1.4,1.1). (a) and (b) are in the moving vortex lattice phase while (c) is in the moving plastic phase.

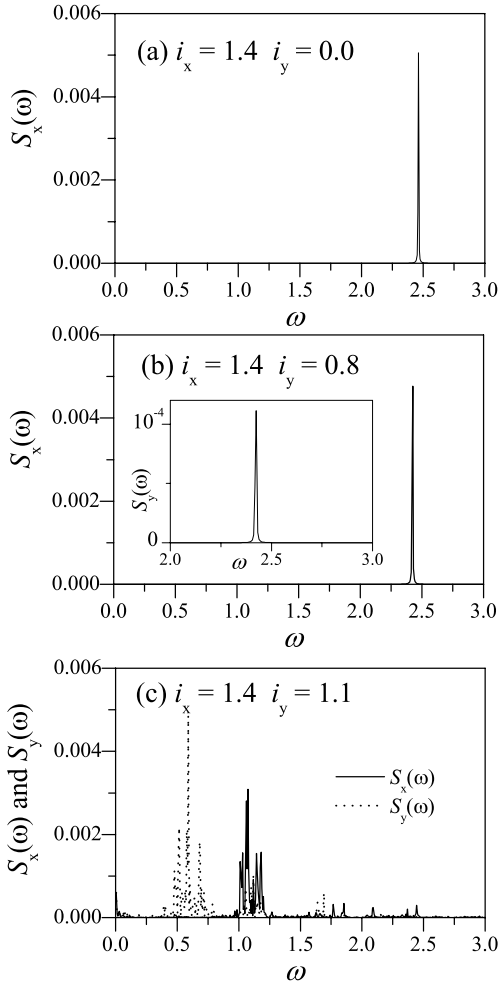

Fig. 5. The voltage power spectra $S_\alpha(\omega)$ ($\alpha = x, y$) for the voltages v_x and v_y at different applied currents as that shown in Figures 4a–c. For the last case with the current **i** = (1.4,1.1), the time-averaged voltages $\langle v_x \rangle$ and $\langle v_x \rangle$ are about 1.14 and 0.636, respectively.

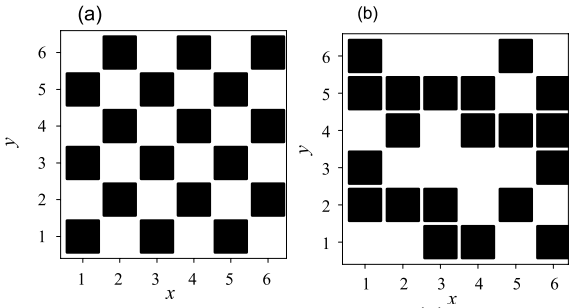

Fig. 6. Typical vortex lattice structure in (a) the moving vortex lattice phase and (b) the plastic phase. Only a 6×6 part of 32×32 arrays is shown. Black squares represent vortices in the system.

corresponding power spectra are exhibited in Figure 5. The trace of the time-dependent voltage $v(t)$ is recorded after the system has reached a steady state. In the moving lattice regime, as shown in Figures 4a and b, the voltage $v_x(t)$ oscillates periodically, and the voltage $v_y(t)$ (if $i_y > 0$) oscillates with exactly the same frequency as v_x but in the opposite phase to v_x, which is quite different from those in reference [6] (*cf.* Figs. 3c and d). Only one peak at the characteristic frequency appears in the power spectra in Figures 5a and b. The frequency of oscillation increases with the current, similar to the RSJ model without frustration [2]. In the moving lattice regime, the vortex lattice move one junction collectively along the y direction step by step, because two vortex lattice configurations with the "checkerboard" pattern which shift one junction are degenerate in the energy. And the vortex lattice moves in phase and the "checkerboard" pattern structure is also kept, see Figure 6a. So the moving lattice phase is characterized by a fundamental angular frequency ω_0, $\omega_0 = \frac{2\pi v_d}{l}$, with v_d the average vortex drift velocity across the sample and $l = 1$ one junction spacing. The mean value of v_x is related to v_d through [37] $\langle v_x \rangle = 2\pi v_d n_f$ with $n_f = 1/2$ the

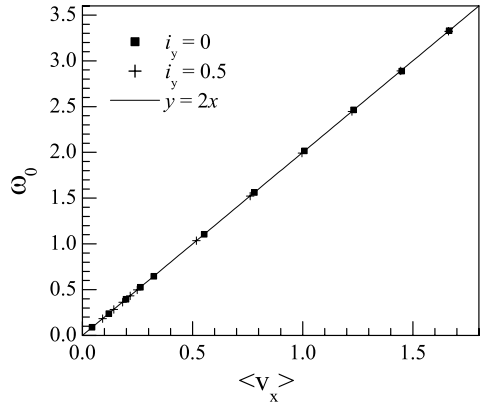

Fig. 7. Dependence of the angular frequency of voltage ω_0 in the moving vortex phase on the time-averaged voltage $\langle v_x \rangle$ for $i_y = 0.0$ and $i_y = 0.5$.

density of vortices in the FF RSJ model. So one readily has

$$\omega_0 = 2\langle v_x \rangle \cdot \tag{10}$$

This relation is also exactly confirmed in Figure 7, where we plot the current dependence of ω_0. The above picture remains valid as long as the system is in the moving lattice regime, due to the absence of the transverse motion even in the presence of a transverse current. It should be stressed here that the frequency in equation (10) is twice that found in reference [6]. We believe that the different behaviors in the time-dependence of the voltage and the power spectrum found in reference [6] can be attributed to the open boundary conditions in current directions, which are less reliable in this problem.

In the plastic flow regime, it might be naively expected that the characteristic frequency would be washed out, as in the random pinning model [25]. Unlike the vortex structure in the moving vortex lattice phase where the vortex lattice keeps its "checkerboard" pattern, the vortex structure in the plastic flow phase is random as shown in Figure 6b. However, at zero-temperature, the effect of lattice pinning plays an important role even in the plastic regime in the present FF RSJ model. Since vortices move in both x and y directions, the vortex spacing is on average twice the grid spacing l. Therefore, besides the dominant plastic flow, motions characterized by angular frequency $\omega_p = \langle v_{x,y} \rangle$ are also possible. As shown in Figure 5c, broad peaks clearly appear around $\omega_p = \langle v_{x,y} \rangle$ and their harmonics for both v_x and v_y. In reference [6], a much more broad peak is also found in this plastic flow (*cf.* Fig. 4a and b), but is not so evident possibly due to either different boundary conditions or the relatively short time of simulations. In our opinion, the effect of the boundary condition becomes weaker in the plastic flow regime, owing to the absence of translational invariant vortex patterns as in the elastic flow regime.

It should be admitted that the results of reference [6] are still valid for small JJA since the finite systems are studied in the OBC.

4 Summary

We have studied the dynamical phase transitions at zero temperature in fully frustrated Josephson junction arrays driven by a current with two orthogonal components. Numerical calculations are carried out for the resistively shunted junction model on the square lattice with the fluctuating twist boundary condition. We find that the time-averaged voltages, as well as the dynamical phase diagram, are almost independent of the lattice size. Three dynamical phases have been observed: a pinned vortex lattice phase, a moving vortex lattice phase and a plastic phase. We find a direct dynamic phase transition from the pinned vortex phase to the moving vortex phase and the separation of the pinned vortex phase and the moving plastic phase, which differ from that observed in systems with open boundary conditions [6]. In the moving lattice phase, the time-dependent voltage is periodic in time and the characteristic angular frequency of the voltage is twice the time-averaged voltage $\omega_0 = 2\langle v \rangle$. The effect of lattice pinning plays an important role even in the plastic regime in the present FF RSJ model. A broad peak is present around a characteristic angular frequency $\omega_p = \langle v \rangle$. A non-monotonic characteristic as well as a hysteresis in IV curves are also found in the plastic regime.

This work was supported by the National Natural Science Foundation of China under Grant No. 10075039 and in part by Ministry of Science and Technology of China (Project No NKBRSF-G1999064602). One of us (M.B.L) gratefully acknowledges support from the National Natural Science Foundation of China under Grant No. 20204014.

References

1. H.S.J. van der Zant, H.A. Zant, H.A. Rijken, J.E. Mooij, J. Low Temp. Phys. **79**, 289 (1990); D.C. Harris, S.T. Herbert, D. Stroud, J.C. Garland, Phys. Rev. Lett. **67**, 3606 (1991); T.K. Shaw, M.J. Ferrari, L.L. Sohn, D.-H. Lee, M. Tinkham, J. Clarke, Phys. Rev. Lett. **76**, 2551 (1996)
2. J.S. Chung, K.H. Lee, D. Stroud, Phys. Rev. B **40**, 6570 (1989)
3. W. Yu, K.H. Lee, D. Stroud, Phys. Rev. B **47**, 5906 (1993)
4. D. Domínguez, Phys. Rev. Lett. **72**, 3096 (1994)
5. M. Franz, S. Teitel, Phys. Rev. Lett. **73**, 480 (1994); Phys. Rev. B **51**, 6551 (1995)
6. K.D. Fisher, D. Stroud, L. Janin, Phys. Rev. B **60**, 15371 (1999)
7. J.P. Straley, E.B. Kolomeisky, Phys. Rev. B **61**, 92 (2000)
8. V.I. Marconi, D. Domínguez, Phys. Rev. Lett. **87**, 17004 (2001)
9. P. Minnhagen, Rev. Mod. Phys. **59**, 1001 (1987)
10. M.S. Rzchowski, L.L. Sohn, M. Tinkham, Phys. Rev. B **43**, 8682 (1991)
11. K.H. Lee, D. Stroud, S.M. Girvin, Phys. Rev. B **48**, 1233 (1993)
12. D. Domínguez, Phys. Rev. Lett. **82**, 181 (1999)
13. B.J. Kim, Phys. Rev. B **63**, 24503 (2000)

14. L.M. Jensen, B.J. Kim, P. Minnhagen, Europhys. Lett. **49**, 644 (2000)
15. V.I. Marconi, D. Domínguez, Phys. Rev. Lett. **82**, 4922 (1999)
16. V.I. Marconi, D. Domínguez, Phys. Rev. B **63**, 174509 (2001)
17. K. Wan, A.K. Jain, J.E. Lukens, Appl. Phys. Lett. **54**, 1805 (1989)
18. G. Filatrella, J. Appl. Phys. **78**, 1878 (1995)
19. B.R. Trees, D. Stroud, Phys. Rev. B **59**, 7108 (1999)
20. G. Blatter, M.V. Feigel'man, V.B. Geshkenbein, Rev. Mod. Phys. **68**, 1125 (1994)
21. S. Bhattacharya, M.J. Higgins, Phys. Rev. B **52**, 64 (1995)
22. M.J. Higgins, S. Bhattacharya, Physica C **257**, 232 (1996)
23. M.C. Faleski, M.C. Marchetti, A.A. Middleton, Phys. Rev. B **54**, 12427 (1996)
24. S. Ryu, M. Hellerqvist, S. Doniach, A. Kapitulnik, D. Stroud, Phys. Rev. Lett. **77**, 5114 (1996)
25. C.J. Olson, C. Reichhardt, F. Nori, Phys. Rev. Lett. **81**, 3757 (1998)
26. T. Giamarchi, P. Le Doussal, Phys. Rev. Lett. **76**, 3408 (1996); P. Le Doussal, T. Giamarchi, Phys. Rev. B **57**, 11356 (1998)
27. K. Moon, R.T. Scalettar, G.T. Zimányi, Phys. Rev. Lett. **77**, 2778 (1996); C.J. Olson, C. Reichhardt, Phys. Rev. B **61**, R3811 (2000)
28. S. Teitel, C. Jayaprakash, Phys. Rev. Lett. **51**, 1999 (1983)
29. S.P. Benz, M.S. Rzchowski, M. Tinkham, C.J. Lobb, Phys. Rev. B **42**, 6165 (1990)
30. B.J. Kim, P. Minnhagen, Phys. Rev. B **60**, 588 (1999); *ibid*, **61**, 7017 (2000)
31. P. Olsson, Phys. Rev. B **46**, 14598 (1992); **52**, 4511 (1995); **52**, 4526 (1995)
32. B.J. Kim, P. Minnhagen, P. Olsson, Phys. Rev. B **59**, 11506 (1999)
33. Q.-H. Chen, L.-H. Tang, P. Tong, Phys. Rev. Lett. **87**, 67001 (2001)
34. A. Petraglia, G. Filatrella, G. Rotoli, Phys. Rev. B **53**, 2732 (1996)
35. J. Holzer, R.S. Newrock, C.J. Lobb, T. Aouaroun, S.T. Herbert, Phys. Rev. B **63**, 184508 (2001)
36. C.J. Olson, C. Reichhardt, Phys. Rev. B **61**, R3811 (1999)
37. C.J. Lobb, D.W. Abraham, M. Tinkham, Phys. Rev. B **27**, 150 (1983)